

**IEEE copyright notice:**

“© © 2012 IEEE. Personal use of this material is permitted. Permission from IEEE must be obtained for all other uses, in any current or future media, including reprinting/republishing this material for advertising or promotional purposes, creating new collective works, for resale or redistribution to servers or lists, or reuse of any copyrighted component of this work in other works.”

**IEEE published version:**

doi:10.1109/ICSMC.2012.6377889

# Identification and Validation of Lateral Driver Models on Experimentally Induced Driving Behavior

Peter Hermannstädter and Bin Yang

Institute of Signal Processing and System Theory, University of Stuttgart, Stuttgart, Germany

{peter.hermannstaedter, bin.yang}@iss.uni-stuttgart.de

**Abstract**—This paper presents a real-world driving experiment with aim on controlled variation of steering and lane keeping behavior and investigates the ability of three common driver models to distinguish variations in driving performance. Nine drivers executed a lane keeping task with visual occlusion of the upper or lower field of view restraining them to near or far road scene information. Three common driver models are applied to replicate driving behavior. An autoregressive model with exogenous input (ARX) is identified using vehicle lateral lane deviation as input and steering wheel angle as output. Two output error models are identified using vehicle heading deviation angles with respect to near and far preview points as respective inputs and steering wheel angle as output. The results show that the driving behaviors induced in the experiment are significantly different in terms of lane keeping performance. In simulations, the output error models exhibit advantages over the ARX model in capturing driving behavior. However, the model natural frequency and the model simulation error show weak performance in discerning this varying driving behavior and are largely determined by track effects.

**Index Terms**—Driver modeling, System identification, Lane keeping, Visual control, Driver monitoring, Fatigue, Intelligent vehicles, Vehicle safety, Driver state

## I. INTRODUCTION

Driver assistance systems increasingly rely on individual characteristics of drivers to optimally support current driving behavior. Conventional calibration of vehicle safety systems in the development phase often involves trade-offs in comfort or efficiency and inherent compromises to suit a variety of drivers. In contrast, online adaptation of safety systems, like driver drowsiness or inattention detection, can improve prevention, interaction and personalization strategies by adjusting system thresholds and parameters to a driver's individual mid-term behavior. This driver behavior can be characterized using driver models.

Driver models can generally be described as adaptive multiple-input multiple-output systems, which focus on replicating a certain driving behavior. Depending on research discipline and application, a large variety of human operator models has been proposed. Due to the vast amount of literature, only a few key references shall be mentioned here. [1]–[5] give good introductions. Models involving psycho-physiological aspects of human behavior have been proposed to increase a priori validity of modeling [6]–[8]. Emphasis on perceptual aspects of driver modeling can be found in [9]. [10] and [11] carry out a system modeling without assumptions about driver psycho-physiology.

This paper refers to two essentially different approaches in [9] and [10]. The first is an approach motivated from human perception, which incorporates a two-point visual control model of the driver. The inputs are deviation angles from vehicle heading to the directions of experimentally determined preview points. [10] suggests a signal-theoretic approach using autoregressive models with exogenous input (ARX) as driver models for detecting driver impairment. Here, model estimation is done from vehicle lateral lane deviation as input and steering wheel angle as output. However, both [9] and [10] are based on driving simulator studies.

Application of driver models to real-world driving data, even when limited to highway driving, imposes increasing challenges. Real-world driving typically shows a large variation in the driving task and driver behavior due to different driving maneuvers, as well as traffic and road conditions. This contradicts the generally limited scope of application of driver models and therefore restricts their description capability.

In order to apply driver models to real driving behavior with minimal disturbances and well-defined variations, this paper is based on driving data collected on a test track in controlled driving experiments. In a lane keeping task, upper and lower regions of the drivers' visual fields were occluded to induce different lateral control behavior of drivers. This paper presents the experiment and investigates the capability of driver models to capture the different driving behaviors in the recorded data.

The driver models applied in this paper are presented in section II-A together with the computation of the preview angle input in section II-B. Section II-C introduces the applied system identification techniques. The conducted driving experiment is introduced in section III. Section IV comprises findings for the experiment setting (IV-A), the results for the identification (IV-B) and evaluation of driver models (IV-C).

## II. DRIVER MODELS

### A. Driver Models with Lateral Offset and Preview Input

In the vehicle-driver system, the driver acts as a regulator in the feedback loop. This system can be sampled in the time domain and transformed into the generic discrete-time system in Figure 1 such that the driver is represented by the dynamics model  $G(q)$ . The vehicle is represented by the feedback model  $K(q)$ .  $H(q)$  is a noise model comprising unmodeled effects and disturbances to the driver-vehicle system. The system's

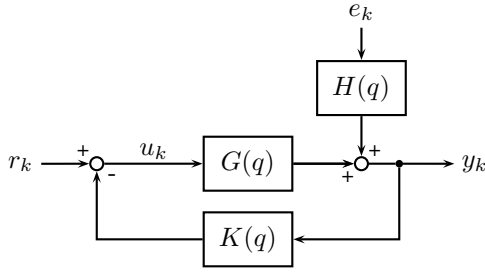


Fig. 1. General system structure with driver model  $G(q)$ , vehicle model  $K(q)$  and noise model  $H(q)$

time difference equations are

$$\begin{aligned} y_k &= G(q)u_k + H(q)e_k \\ u_k &= r_k - K(q)y_k \end{aligned}$$

where  $r_k$  is a generic environment reference,  $u_k$  resembles the control error perceived by the driver,  $y_k$  is the measured driver control output and  $e_k$  is sampled white noise.  $q$  is the one step time shift operator such that  $q^{-1}x_k = x_{k-1}$ .

Among the large number of driver models, we first concentrate on the approach in [10], which is then developed into a preview driver model with human perception characteristics. The driver model is obtained by fitting a second-order ARX model to simulator data using least-squares estimation. The vehicle's measured lateral offset  $d_k$  from the lane center as depicted in Figure 2(a) is used as input and the steering wheel angle  $\delta_k$  as output. This lateral offset model is denoted as  $G_{\text{lat}}(q)$  with the specific input and output signals  $u_k = d_k$ ,  $y_k = \delta_k$ .

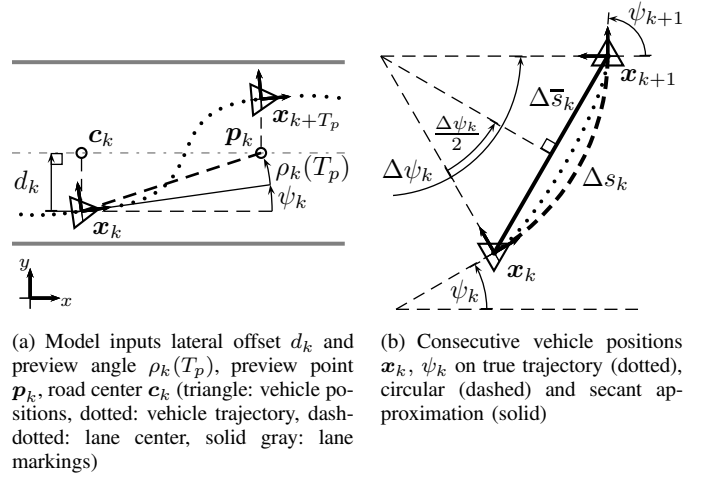
Considering the model input  $d_k$ , it is obvious that in practice the current lateral lane deviation of the vehicle is hard to perceive for the driver. Hence, this model does not reflect the true driver behavior well. Drivers are more likely to use information from the road scene ahead of the vehicle. In the second model, the concept of preview points and preview angles from [9] is used instead. The input is now the angular deviation  $\rho_k(T_p)$  between the vehicle's heading and a preview point  $\mathbf{p}_k = [p_{x,k} \ p_{y,k}]^T$  in the center of the road at a given preview time  $T_p$ , as shown in Figure 2(a). The output is again the steering wheel angle  $\delta_k$ . This preview point model is denoted by  $G_{\text{pre}}(q)$  with the specific signals mapping  $u_k = \rho_k(T_p)$ ,  $y_k = \delta_k$ .

As in [10], we assume that both  $G_{\text{lat}}(q)$  and  $G_{\text{pre}}(q)$  can be represented as second-order rational functions of  $q$  and a parameter vector  $\theta$

$$G(q, \theta) = \frac{B(q, \theta)}{A(q, \theta)} = \frac{b_1 q^{-1} + b_2 q^{-2}}{1 + a_1 q^{-1} + a_2 q^{-2}}. \quad (2)$$

For the two models above,  $\theta_{\text{lat}}$  and  $\theta_{\text{pre}}$  are defined by

$$\begin{aligned} \theta_{\text{lat}} &= [a_{\text{lat},1} \ a_{\text{lat},2} \ b_{\text{lat},1} \ b_{\text{lat},2}]^T \\ \theta_{\text{pre}} &= [a_{\text{pre},1} \ a_{\text{pre},2} \ b_{\text{pre},1} \ b_{\text{pre},2}]^T. \end{aligned}$$



(a) Model inputs lateral offset  $d_k$  and preview angle  $\rho_k(T_p)$ , preview point  $\mathbf{p}_k$ , road center  $\mathbf{c}_k$  (triangle: vehicle positions, dotted: vehicle trajectory, dash-dotted: lane center, solid gray: lane markings)

(b) Consecutive vehicle positions  $\mathbf{x}_k, \psi_k$  on true trajectory (dotted), circular (dashed) and secant approximation (solid)

Fig. 2. Model inputs and approximation of vehicle and lane trajectory

### B. Calculation of the Preview Angle

Available vehicle data comprises steering wheel angle  $\delta_k$ , vehicle speed  $v_k$ , yaw rate  $\dot{\psi}_k$  and current lateral offset  $d_k$  from the lane center, all sampled at a sampling interval  $T_s = 0.02$  s with off-the-shelf vehicle sensors.

Whereas the lane deviation  $d_k$  is directly measured, the preview angle  $\rho_k(T_p)$  and the preview point  $\mathbf{p}_k$  are unknown and have to be calculated from the vehicle and the lane trajectory. For reconstruction of the vehicle trajectory, the vehicle motion is approximated as circular motion during a sampling interval  $T_s$ . In Figure 2(b), the dotted vehicle path of length  $T_s v_k$  is first approximated by the circle arc length  $\Delta s_k \approx T_s v_k$  (dashed) spanning the angle  $\Delta \psi_k = \psi_{k+1} - \psi_k \approx T_s \dot{\psi}_k$  and second by the secant  $\Delta s_k \approx \Delta \bar{s}_k$  (solid). The vehicle trajectory  $\mathbf{x}_k$  in the inertial coordinate frame is reconstructed as

$$\begin{aligned} \psi_k &= \psi_{\text{ic}} + \sum_{i=0}^{k-1} T_s \dot{\psi}_i \\ \mathbf{x}_k &= \mathbf{x}_{\text{ic}} + \sum_{i=0}^{k-1} \underbrace{\begin{bmatrix} \cos \psi_i & -\sin \psi_i \\ \sin \psi_i & \cos \psi_i \end{bmatrix}}_{\mathbf{R}(\psi_i)} \begin{bmatrix} \Delta s_i \cos \frac{\Delta \psi_i}{2} \\ \Delta s_i \sin \frac{\Delta \psi_i}{2} \end{bmatrix} \end{aligned}$$

with rotation matrix  $\mathbf{R}(\psi_i)$  from vehicle to inertial frame and starting from some initial conditions  $\psi_{\text{ic}}, \mathbf{x}_{\text{ic}}$ .

The lateral offset  $d_k$  of the vehicle from the lane center is measured relative to  $\mathbf{x}_k$  and perpendicular to the lane, as in Figure 2(a). Assuming small relative yaw angles of the vehicle with respect to the lane, the lane center position is in the inertial frame

$$\mathbf{c}_k = \mathbf{x}_k + \mathbf{R}(\psi_i) \begin{bmatrix} 0 \\ -d_k \end{bmatrix}.$$

The preview point  $\mathbf{p}_k$  is now determined at  $T_p$  ahead of the vehicle under the assumptions that during  $T_p$  the vehicle remains within the lane boundaries and its speed approximately constant. Then,  $T_p$  can be measured in integer multiples of  $T_s$  along the driven trajectory until  $\mathbf{x}_{k+T_p}$  with good approximation. Consequently, it is  $\mathbf{p}_k = \mathbf{c}_{k+T_p}$  the lane center at

$k + T_p$ , which corresponds to a simple time shift and simplifies computations. For a given preview time, the preview point relative to the vehicle is  $\mathbf{p}_k^v = \mathbf{R}^{-1}(\psi_i)(\mathbf{p}_k - \mathbf{x}_k)$  and the preview angle is given by

$$\rho_k(T_p) = \tan^{-1} \left( \frac{p_{y,k}^v}{p_{x,k}^v} \right) \quad \left| \rho_k(T_p) \right| < \frac{\pi}{2}. \quad (3)$$

### C. Identification of Driver Model Parameters

Identifying parameters of the model (2) from data recorded in the closed-loop setting of Figure 1 imposes difficulties on consistent parameter estimation [12], because the noise  $e_k$  and the input  $u_k$  are correlated due to feedback  $K(q)$ . Since the true  $K(q)$  and  $H(q)$  are unknown, quantification of these influences is inaccurate. Therefore, assuming a small contribution of feedback to  $u_k$  or a good signal-to-noise ratio (SNR) of  $u_k$  and  $e_k$  [12], the correlation of input and noise due feedback is neglected. The estimation problem for  $G(q)$  thus simplifies to an open-loop estimation from  $u_k$  and  $y_k$ .

In [10], the driver model is obtained by fitting the ARX model to driving simulator data using least-squares estimation. The implied system model is

$$\begin{aligned} A(q) y_k &= y_k + a_1 y_{k-1} + a_2 y_{k-2} \\ &= B(q) u_k = b_1 u_{k-1} + b_2 u_{k-2} + e_k. \end{aligned}$$

For  $G_{\text{lat}}(q, \theta)$ , the lane lateral deviation  $u_k = d_k$  is used as model input and the steering wheel angle  $y_k = \delta_k$  as output. This model can be written as a linear regression

$$\begin{aligned} y_k &= [y_{k-1} \quad y_{k-2} \quad u_{k-1} \quad u_{k-2}] \theta + e_k \\ &= \phi_k^T \theta + e_k \end{aligned}$$

with the vector of regressors  $\phi_k$ . Note that  $\phi_k$  contains no previous prediction values and thus the prediction error  $\epsilon_k(\theta) = y_k - \hat{y}_k$  of model  $G_{\text{lat}}(q, \theta)$  is the one-step prediction error

$$\epsilon_k(\theta) = y_k - G_{\text{lat}}(q, \theta) u_k = y_k - \phi_k^T \theta. \quad (4)$$

The estimate  $\hat{\theta}$  of the parameters is obtained by solving

$$\hat{\theta} = \arg \min_{\theta} V(\theta) \quad (5)$$

where  $V$  is the mean square error (MSE) of the prediction

$$V(\theta) = \frac{1}{N} \sum_{k=1}^N \epsilon_k^2(\theta). \quad (6)$$

The solution is  $\hat{\theta}_{\text{lat}} = \hat{\theta} = (\Phi^T \Phi)^{-1} \Phi^T \mathbf{y}$ , where  $\Phi$  is the  $N \times 4$  matrix of regressors  $\Phi = [\phi_k \dots \phi_{k-N+1}]^T$ .

The implied noise model is  $H(q, \theta) = 1/A(q)$  due to

$$y_k = \frac{B(q)}{A(q)} u_k + \frac{1}{A(q)} e_k = G(q, \theta) u_k + H(q, \theta) e_k.$$

This facilitates a direct analytical solution of (5). However, least-squares estimation of  $G(q)$  and  $H(q)$  emphasizes a fit to high frequency components in the data [13]. This is undesirable, since the relevant frequencies in manual control tasks range only up to about 5 rad/s as stated in [14]. Moreover,

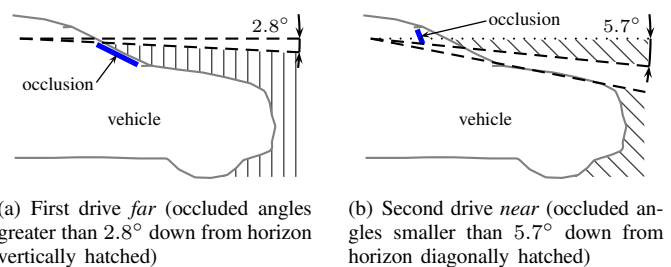


Fig. 3. Field of view occlusions setups

in real-world driving with numerous disturbances, the noise model is unlikely to be accurately described by  $H(q, \theta) = 1/A(q)$ .

As an improvement, [12] suggests, under the above simplification to an open-loop scenario, an *output error* identification using the system model

$$y_k = \frac{B(q)}{A(q)} u_k + e_k$$

with  $H(q) = 1$ . In addition, we use the preview angle  $u_k = \rho_k(T_p)$  from (3) for a given preview time  $T_p$  as system input and the steering wheel angle  $y_k = \delta_k$  as system output for  $G_{\text{pre}}(q, \theta)$ .

The prediction  $\hat{y}_k = G_{\text{pre}}(q, \theta) u_k$  with this system model is recursive and depends on previous predictions  $\hat{y}_{k-1}, \hat{y}_{k-2}$ . Thus, instead of the one-step prediction error from (4), identification is here based on the  $N$ -step simulation error

$$\tilde{\epsilon}_k(\theta) = y_k - \hat{y}_k = y_k - G_{\text{pre}}(q, \theta) u_k.$$

The model  $G_{\text{pre}}(q, \theta)$  is therefore evaluated in a simulation over multiple steps, which improves capturing the dynamics of the true process. Similar to (5) and (6), the minimization problem is formulated as

$$\hat{\theta} = \arg \min_{\theta} \tilde{V}(\theta) = \arg \min_{\theta} \frac{1}{N} \sum_{k=1}^N \tilde{\epsilon}_k^2(\theta).$$

where  $\tilde{V}(\theta)$  is the simulation MSE and an iterative solution yields the parameter estimate  $\hat{\theta}_{\text{pre}} = \hat{\theta}$ .

This paper makes use of Ljung's *System Identification Toolbox* for *MATLAB*, solving output error problems with problem-specific iterative techniques together with estimation of optimal initial conditions for the model (see [12]).

### III. EXPERIMENT SETUP

Controlled experiments with a range of windshield occlusions have been conducted to record the driver steering and lane keeping performance and suppress disturbances at large. Nine male expert drivers were recruited to complete three drives of a lane keeping task.

For the first and the second of the three drive tasks, the driver's field of view was restricted in vertical angular direction. During the first drive, only visual information in the area of viewing angles smaller than 2.8 degrees down from the horizon was available. This corresponded to minimum viewing

distances of approximately 24 m. Occlusion corresponding to the vertically hatched area in Figure 3(a) was achieved by partially covering the vehicle’s windshield.

During the second drive, only viewing angles greater than  $5.7^\circ$  down from the horizon were visible, what corresponded to a maximum viewing distance of approximately 12 m. Occlusion corresponding to the diagonally hatched area in Figure 3(b) was accomplished using the vehicles standard sun visor.

The third drive was executed as a reference drive without visual occlusion.

For the calibration of the occlusion settings, the vehicle was placed in a well-defined position. The subjects were told to adjust their seat in order to match their line of sight with the occlusion edge and calibration marks outside the vehicle. In order to maintain the calibrated field of view, the drivers were instructed to recline the back of their head on the driver seat’s head rest at all times.

For all drives, the subjects were instructed to steer the vehicle in the middle of the lane. The drives were carried out on a rural road test track consisting of a launch area up to 0.3 km, a successive  $0^\circ$  flat straight section of approximately 1.7 km and a curved section of 1.1 km with right-only curve radii varying from 0.4 km over 0.3 km to 0.2 km. The drives were carried out with cruise control set to 80 km/h on the right of two one-way lanes. The subjects had prior knowledge about the track.

All drives were carried out using a Mercedes-Benz E class vehicle and accompanied by a trained expert driver<sup>1</sup>.

In the following, the test drives are labeled according to the visible field of view with *far* for visible far-region field of view (first drive, Fig. 3(a)), *near* for visible near-region field of view (second drive, Fig. 3(b)) and with *ref* for the unoccluded reference drive, respectively. Moreover, within the drives, the first track sections on the straight are labeled as *straights* and the curved track sections as *curves*.

#### IV. RESULTS

Processing of experiment data is only performed after rejection of disturbed drive data with introductory and final lane changes, vehicle speeds below 60 km/h or invalid lane tracking signals. All models and analyses are applied to moving windows of  $N = 200$  (4 seconds) samples of the vehicle and lane trajectory data from II-B with a window shift of 50 samples (1 second).

##### A. Experiment and Driving Behavior

The driving behaviors induced by the occlusion drives and the reference drive are evaluated using the standard deviation of lateral offset, a common driving performance measure. The sample standard deviation  $\sigma_{d,N}$  of  $d_k$  is computed for each window. Figure 4 shows a box and whisker plot of  $\sigma_{d,N}$  grouped by drives. The influence of track segments is disregarded in view of similar tendencies. The three runs with far-region perspective *far*, near-region perspective *near* and reference *ref* result in significantly different driving behaviors

<sup>1</sup>Experiment and data courtesy of Daimler AG.

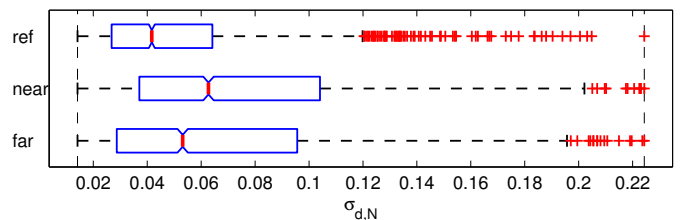


Fig. 4. Lateral offset standard deviation  $\sigma_{d,N}$  for respective drives *ref*, *near* and *far* (box range: 25th to 75th percentile; median: red bar; notches: 95% confidence interval of median; whiskers: 1.5 times interquartile range; outliers: “+”; dashed lines: clipping to 95% of data for visualization)

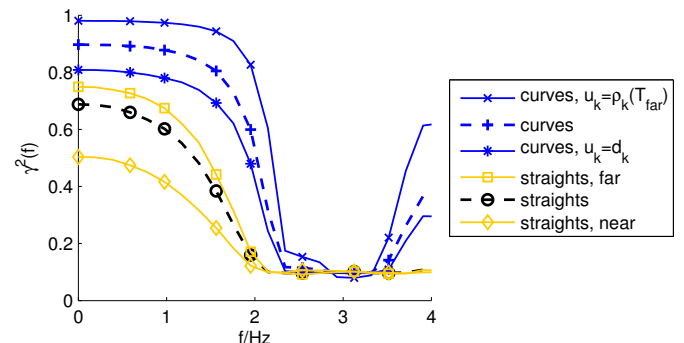


Fig. 5. Medians of coherence function  $\gamma^2(f)$  in relevant frequency range

over all drivers, since in Figure 4, each confidence interval (CI) notch contains only its group’s median (in particular: Kruskal-Wallis test  $p \ll 0.001$ ).

##### B. Driver Model Identification

The model  $G_{\text{lat}}(q, \theta)$  and two variants of  $G_{\text{pre}}(q, \theta)$  are applied to the data. For the two occlusion setups *far* and *near*, respective preview times are calculated using the vehicle reference speed and the respective minimum and maximum viewing distances (see section III) such that

$$\text{1st drive, far field view: } T_{\text{far}} = 1.08 \text{ s,}$$

$$\text{2nd drive, near field view: } T_{\text{near}} = 0.54 \text{ s.}$$

Two corresponding preview point inputs  $\rho(T_{\text{far}})$  and  $\rho(T_{\text{near}})$  are computed according to section II-B.

Thus, the driver models analyzed in the following are

$$\text{lateral offset: } \hat{\delta}_{\text{lat},k} = \hat{G}_{\text{lat}}(q) d_k, \quad (7a)$$

$$T_{\text{far}} \text{ preview: } \hat{\delta}_{\text{pre, far},k} = \hat{G}_{\text{pre, far}}(q) \rho_k(T_{\text{far}}), \quad (7b)$$

$$T_{\text{near}} \text{ preview: } \hat{\delta}_{\text{pre, near},k} = \hat{G}_{\text{pre, near}}(q) \rho_k(T_{\text{near}}). \quad (7c)$$

For linearity check of the model input-output pairings in (7), the coherence function  $\gamma^2(f)$  [12] – the normalized cross-correlation function in the frequency domain – is computed for every data window. Figure 5 depicts a low-frequency section of the medians over all windows of  $\gamma^2(f)$  for selected track and input combinations.  $\gamma^2(f) \approx 1$  corresponds to high linearity and  $\gamma^2(f) \approx 1$  to low linearity at a frequency  $f$ . Comparing  $u_k = \rho_k(T_{\text{far}})$  and  $u_k = d_k$ , it is notable that the

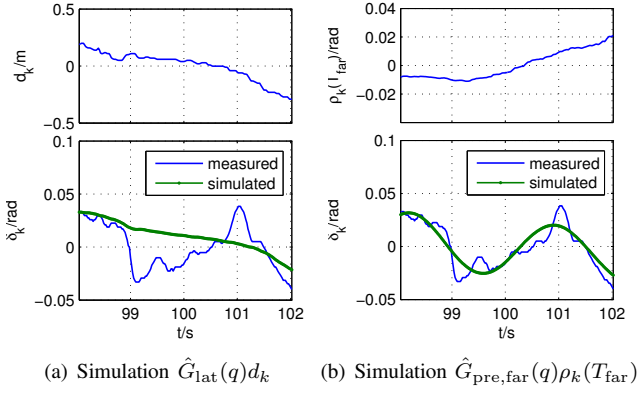


Fig. 6. Exemplary input-output data and model simulations ( $t = kT_s$ )

choice of  $T_p$  influences linearity. This may be due to delay and acausality effects introduced by improper preview times when modeling a previewing driver. Track segments, however, have greater influences on linearity as shown by the large difference between the median of  $\gamma^2(f)$  for *curves* and for *straights*. The occlusion setting also influences linearity in that with decreasing viewing distance from *far* to *near* linearity degrades, as shown here for *straights*. So-called complacency [10] may account for nonlinearity by perception thresholds on or negligence of small control errors, particularly when excitation by the reference signal is low as on *straights*. Moreover, disturbances then have a comparatively large impact and the SNR is poor. For identification of driver models, linear model estimation is justified:  $\gamma^2(f)$  shows sufficient linearity for the relevant frequencies up to  $0.8 \text{ Hz} \approx 5 \text{ rad/s}$  [14].

For every window, after subtraction of its mean, ARX and output error identification are conducted resulting in the models  $\hat{G}_{\text{lat}}(q)$ ,  $\hat{G}_{\text{pre, near}}(q)$ ,  $\hat{G}_{\text{pre, far}}(q)$ , respectively. Figure 6 shows an exemplary data window and predicted responses of an ARX model  $\hat{G}_{\text{lat}}(q)$  and a  $T_{\text{far}}$  preview model  $\hat{G}_{\text{pre, far}}(q)$  both identified from the depicted input-output data.

The upper plots show the input data with lane deviation  $d_k$  and preview angle  $\rho_k(T_{\text{far}})$ , respectively. The lower plots depict the measured steering wheel angle  $\delta_k$ , as well as the simulated steering wheel angle over the depicted window using the model in (7a) and (7b). Comparing Figures 6(a) and 6(b), the benefits of the output error approach for driver model identification are obvious.

### C. Evaluation and Comparison of Driver Model

A validity measure is constructed, such that identified driver models are only evaluated if they are stable, the identification residuals  $\epsilon_k(\hat{\theta}_{\text{lat}})$  and  $\tilde{\epsilon}_k(\hat{\theta}_{\text{pre}})$  are independent of the model input in terms of temporal correlation and the model fit in terms of percentage of explained variance is nonnegative [12]. Moreover the respective identification MSEs  $V(\hat{\theta}_{\text{lat}})$  and  $\tilde{V}(\hat{\theta}_{\text{pre}})$  are required to be sufficiently small ( $V(\hat{\theta}_{\text{lat}}), \tilde{V}(\hat{\theta}_{\text{pre}}) < 10^{-3}$ ). In total, 2230 models  $\hat{G}_{\text{lat}}(q)$ , 1374 models  $\hat{G}_{\text{pre, near}}(q)$  and 1292 models  $\hat{G}_{\text{pre, far}}(q)$  are valid and analyzed in the following.

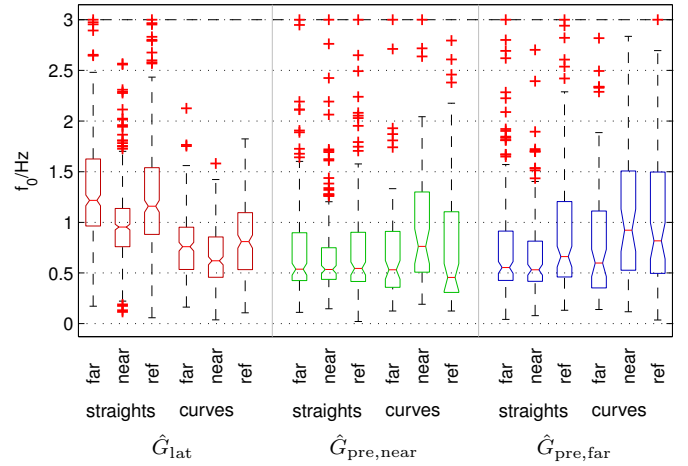


Fig. 7. Distributions of natural frequencies  $f_0$  with respect to driver field of view and drive segments

The performance of driver models to describe the driver behavior is evaluated using natural frequency and cross-validation simulation residuals.

For calculating the natural frequency, the poles  $z_n$  of the denominator polynomial  $\hat{A}(z)$  of discrete-time transfer function representation  $\hat{G}(z)$  of  $\hat{G}(q)$  are determined. Transformation of  $z_n$  to time-continuous equivalents  $s_n = \ln(z_n)/T_s$  and subsequent polynomial expansion yields the denominator polynomial  $\hat{A}_n(s)$  of the continuous-time transfer function representation  $\hat{G}_n(s)$  [10]. The natural frequencies  $f_0 = \omega_0/2\pi$  are extracted for every window and all identified models from

$$\hat{A}(s) = s^2 + 2\zeta_n\omega_0 s + \omega_0^2.$$

Figure 7 depicts the distributions of  $f_0$  in groups. As an overall result, the natural frequencies of  $\hat{G}_{\text{lat}}(q)$  provide weak discrimination of the occlusion settings. However, for  $\hat{G}_{\text{pre, near}}(q)$  and  $\hat{G}_{\text{pre, far}}(q)$  the notch intervals overlap and thus no distinction is possible using natural frequencies of these models. A major reason for this are the smaller numbers of valid output error models resulting in less certain median CIs and thus larger notch intervals. Moreover,  $f_0$  shows major dependency on the track segments *straight* and *curve*.

A different approach to assess driver models and driver behavior uses the simulated responses of the identified driver model instead of exploiting its parameters [10]. For all models  $\hat{G}_{\text{lat}}(q)$ ,  $\hat{G}_{\text{pre, near}}(q)$  and  $\hat{G}_{\text{pre, far}}(q)$ , the simulation MSEs  $\tilde{V}(\hat{\theta}_{\text{lat}})$ ,  $\tilde{V}(\hat{\theta}_{\text{pre, near}})$  and  $\tilde{V}(\hat{\theta}_{\text{pre, far}})$  are computed in a cross-validation approach adopted from [11]. The models are identified from a window of input-output data and are simulated on the successive window partly containing previously unseen data. The resulting cross-validation simulation MSEs are depicted in Figure 8 in logarithmic scale. Within a track segment, all models show comparable performance. Discerning the occlusion setting *near* from *far* and from *ref* is possible with significance with all models on *straights*, since the notch intervals are distinct. This doesn't hold for the distinction of *far* and *ref* and fails to become significant for *curves*, where only

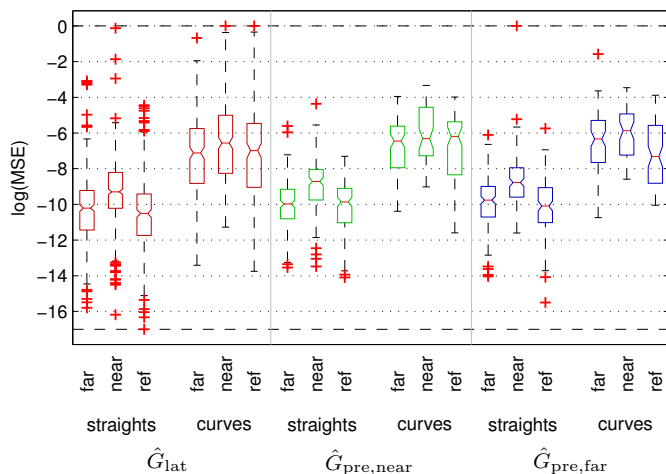


Fig. 8. Cross-validation simulation MSEs (outliers clipped at dashed line)

the  $\hat{G}_{lat}(q)$  exhibits weak differences in MSE medians. In turn,  $\hat{G}_{lat}(q)$  exhibits larger performance variations in comparison with the output error models. However, the track segments are also a major influence on the overall model performances in cross-validation. The MSEs differ by more than two orders of magnitude between *curves* and *straights* thus outweighing driving behavior effects.

Comparing Figures 7 and 8, the cross-validation MSEs exhibit slight advantages compared to the natural frequencies in terms of discrimination of occlusion settings. Moreover, it can be observed that the MSEs of the output error models show a smaller number of outliers and more regular distributions compared to the MSE of the model  $\hat{G}_{lat}(q)$  and the distributions of natural frequency in Figure 7.

## V. DISCUSSION AND FUTURE WORK

The driving experiment presented in this paper successfully constituted significantly different driving behaviors by partially occluding the driver's upper or lower field of view. The real-world driving data collected under well-defined conditions bridges a gap between measurements in driving simulators and on public roads, but also reveals critical issues for real-world application of driver models.

In capturing driving behavior with driver models, simulations reveal advantages of the output error models over the ARX model. However, in discerning the induced driving behavior, all models show only weak results. Widely, track influences on the models are larger than possible effects from driving behavior. The potentially too simple second-order models reveal no convincing distinctions. The large variations of the model performances within pairings of track segment and occlusion setting may result from unmodeled dynamics and nonlinearities in the driver, but also from disturbance effects, e.g. road surface or vehicle nonlinearities. In evaluation of the driver models, neither natural frequency nor simulation MSE reveal clear tendencies, as both suffer from above influences. With fewer outliers and a larger number of distinguished situations, the simulation MSE has slight explanatory advantages

compared to natural frequency. However, the latter is easier to determine as no simulation is needed.

Systematic limitations are imposed by the simplified system identification approach being a first choice during ongoing research. The disregarded feedback effects may introduce estimation bias in case the assumptions of good SNR and small feedback are violated. Moreover, both noise models are potentially oversimplified and likely to misjudge the noise impacts. The recorded data is used in system identification without prefiltering resulting in a model fit to frequencies far above the range relevant for human manual control.

As this paper is part of work in progress on driver modeling and driver state detection, the above limitations and drawbacks are yet to be conquered in order to achieve feasible driver modeling for real-world applications. In further works, special emphasis is put on establishing a closed-loop identification approach. Improvements are expected by identifying an accurate noise model from the data and similarly by prefiltering input-output data to relevant frequency ranges. Due to strong nonlinear effects of misadjusted preview times, additional driver preview strategies and preview preprocessing have to be examined. Further investigation will also consider additional driver models with higher a priori validity and stronger relations to human characteristics.

## REFERENCES

- [1] T. Jürgensohn, "Control Theory Models of the Driver," in *Modelling Driver Behaviour in Automotive Environments*, P. C. Cacciabue, Ed. London: Springer, 2007, pp. 277–292.
- [2] D. H. Weir and K. C. Chao, "Review of Control Theory Models for Directional and Speed Control," in *Modelling Driver Behaviour in Automotive Environments*, P. C. Cacciabue, Ed. London: Springer, 2007, pp. 293–311.
- [3] D. McRuer, "Human dynamics in man-machine systems," *Automatica*, vol. 16, no. 3, pp. 237–253, 1980.
- [4] H.-P. Willumeit and T. Jürgensohn, "Fahrermodelle: ein kritischer Überblick. Teil 1," *ATZ. Automobiltechnische Zeitschrift*, vol. 99, no. 7-8, pp. 424–428, 1997.
- [5] —, "Fahrermodelle: ein kritischer Überblick. Teil 2," *ATZ. Automobiltechnische Zeitschrift*, vol. 99, no. 9, pp. 552–560, 1997.
- [6] F. Mars, L. Saleh, P. Chevrel, F. Claveau, and J.-F. Lafay, "Modeling the Visual and Motor Control of Steering With an Eye to Shared-Control Automation," in *Proc. of the Hum. Fact. and Ergo. Society 55th Annual Meeting*, 2011, pp. 1422–1426.
- [7] S. D. Keen and D. J. Cole, "Steering control using model predictive control and multiple internal models," *AVEC 2006*, 2006.
- [8] A. M. C. Odhams, "Identification of Driver Steering and Speed Control," Ph.D. dissertation, Cambridge University, Cambridge, September 2006.
- [9] D. D. Salvucci and R. Gray, "A two-point visual control model of steering," *Perception*, vol. 33, no. 10, pp. 1233–1248, 2004.
- [10] T. E. Pilutti and A. G. Ulsoy, "Identification of driver state for lane-keeping tasks," *IEEE Transactions on Systems, Man, and Cybernetics, Part A*, vol. 29, no. 5, pp. 486–502, 1999.
- [11] M. Shi, "Real time human driver identification for improved safety," Ph.D. dissertation, University of California, Berkeley, CA, 2008.
- [12] L. Ljung, *System identification : theory for the user*, 29th ed. Upper Saddle River and NJ [u.a.]: Prentice Hall, 2006.
- [13] Y. Tomita, A. A. H. Damen, and P. M. J. van den Hof, "Equation error versus output error methods," *Ergonomics*, vol. 35, no. 5-6, pp. 551–564, 1992.
- [14] G. Johansson, *Der Mensch im Regelkreis: Lineare Modelle*, 1st ed., ser. Methoden der Regelungstechnik. München and Wien: Oldenbourg, 1977.